Inorganic Chemistry

Article

pubs.acs.org/IC

Modulation of Ligand-Field Parameters by Heme Ruffling in Cytochromes *c* Revealed by EPR Spectroscopy

Mehmet Can,[†,§] Giorgio Zoppellaro,[‡,§] K. Kristoffer Andersson,[‡] and Kara L. Bren*[,†]

[†]Department of Chemistry, University of Rochester, Rochester, New York 14627-0216, United States

[‡]Department of Molecular Biosciences, University of Oslo, Post Office Box 1041, Blindern, Oslo NO-0316, Norway

Supporting Information

ABSTRACT: Electron paramagnetic resonance (EPR) spectra of variants of *Hydrogenobacter thermophilus* cytochrome c_{552} (*Ht c*-552) and *Pseudomonas aeruginosa* cytochrome c_{551} (*Pa c*-551) are analyzed to determine the effect of heme ruffling on ligand-field parameters. Mutations introduced at positions 13 and 22 in *Ht c*-552 were previously demonstrated to influence hydrogen bonding in the proximal heme pocket and to tune reduction potential (E_m) over a range of 80 mV [Michel, L. V.; Ye, T.; Bowman, S. E. J.; Levin, B. D.; Hahn, M. A.; Russell, B. S.; Elliott, S. J.; Bren, K. L. *Biochemistry* **2007**, *46*, 11753−11760]. These mutations are shown here to also increase heme ruffling as E_m decreases. The primary effect on electronic structure of increasing heme ruffling is found to be a decrease in the axial ligand-field term Δ/λ, which is proposed to arise from an increase in the energy of the d_{xy} orbital. Mutations at position 7, previously demonstrated to influence heme ruffling in *Pa c*-551 and *Ht c*-552, are utilized to test this correlation between molecular and electronic structure. In conclusion, the structure of the proximal heme pocket of cytochromes *c* is shown to play a role in determining heme conformation and electronic structure.

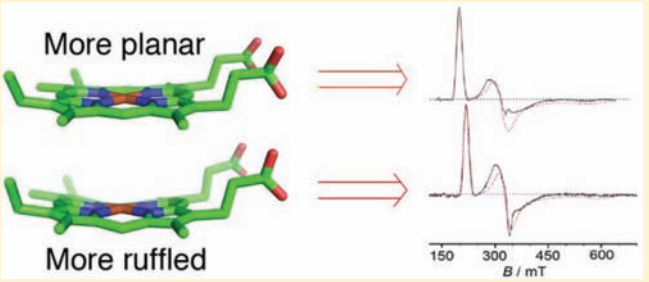

INTRODUCTION

Iron protoporphyrin IX (heme) is a cofactor found in proteins that carry out electron transfer, oxygen transport and storage, sensing, and a wide range of metabolic processes. Heme *c* is a widely distributed form of heme characterized by covalent attachment to two Cys in a Cys-X-X-Cys-His (CXXCH) motif in which His is an axial ligand to the iron of the heme.[1] His/Met is a common ligand set for heme *c* and is seen in soluble cytochromes *c*, photosynthetic reaction centers, mitochondrial cytochromes c_1, diheme cytochrome *c* peroxidases, and several dehydrogenases and cytochrome cd_1 nitrite reductases.[1,2] Analysis of structures of hemes *c* with His/Met axial ligation reveals that the His imidazole ring is generally oriented along the porphyrin $\alpha-\gamma$ meso axis (Figure 1A).[3] The axial Met side chain, in contrast, can adopt a number of orientations relative to the heme plane.[4,5] In some cases, Met fluxionality, a phenomenon that involves rapid interconversion between the *R* and *S* configurations at the Met δS, is observed.[6,7] Although heme proteins with His/Met axial ligation have been studied extensively using a variety of spectroscopic methods, detailed relationships between active-site structure, *g* values, and associated ligand-field components determined by spectroscopic methods such as EPR, Mössbauer, MCD, and NMR remain elusive for this important class of proteins.[8−10]

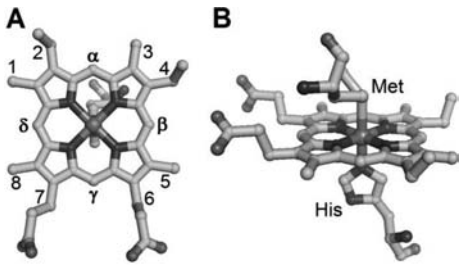

Figure 1. Active-site structure of *Pseudomonas aeruginosa* cytochrome c_{551} (PDB 351C[11]) showing (A) Fisher numbering system and axial His orientation and (B) Met and His axial ligands.

In contrast with heme with His/Met axial ligation, for heme with His/His axial ligation, relationships between heme active-site structure, *g* values, and NMR hyperfine shifts are well-defined.[12−14] In particular, it has been established that the angle between the two axial His imidazole planes plays a major role in determining the *g*-tensor and ligand-field parameters. If the two axial His planes are oriented perpendicular or nearly so to each other, a large g_{max} value ($g_{max} > 3.3$) and an axial EPR spectrum results, whereas a relatively small angle between the axial ligand planes yields a lower g_{max} value and a rhombic spectrum.[12] The spin−orbit coupling constant (λ) and the experimentally observed *g* values can be used to estimate the rhombic (*V*) and axial (Δ) ligand-field terms,[15] and thus the relative energies of the iron(III) d-orbitals (Figure 2); the ratio V/Δ is used as an indicator of the system's rhombicity. The axial His imidazole

Received: July 12, 2011
Published: November 1, 2011

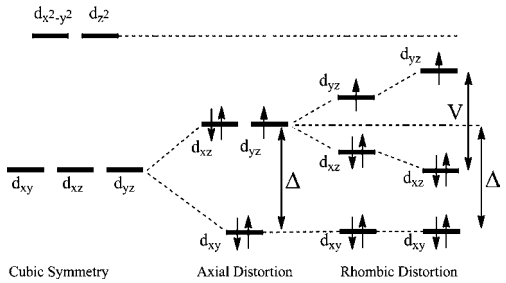

Figure 2. Energy diagram of the d-orbitals for the low-spin ferric heme *c* (S = 1/2) with $(d_{xy})^2(d_{xz})^2(d_{yz})^1$ orbital occupancy. The axial (Δ) and rhombic (V) ligand-field parameters are shown.

plane orientations also correlate with the NMR hyperfine shifts of heme substituents, and thus for proteins with His/His axial ligation, interrelationships among properties of NMR spectra, EPR spectra, and active-site structure are well established.

Progress toward understanding how EPR parameters reflect properties of heme with His/Met axial ligation was made in a study of a series of cytochrome *c* variants in which linear relationships were identified between the average heme methyl chemical shift ($\langle\delta\rangle$) determined from NMR and both g_{max} and V/Δ determined from EPR. A structural basis for the observed changes was not established, but it was proposed to be associated with heme conformation, axial ligand strength and orientation, or a combination of these factors.[9] In the present study, to better define the relationship between molecular and electronic structure of heme *c* with His/Met axial ligands, we report an analysis of EPR data on a series of mutants of small, soluble bacterial cytochromes *c*. The proteins targeted, *Hydrogenobacter thermophilus* cytochrome c_{552} (*Ht c*-552), and *Pseudomonas aeruginosa* cytochrome c_{551} (*Pa c*-551), constitute a homologous pair with 57% sequence identity. Mutations in these proteins have been made at positions 7, 13, and 22, which are located near the CXXCH heme attachment site (residues 12−16; Figure 3). Mutation of residue 7 has been shown to

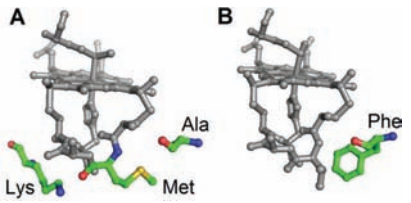

Figure 3. Mutation sites in this study: (A) Ala7, Met13, and Lys22, shown in *Ht c*-552 (PDB 1YNR[20]) (B) Phe7, shown in *Pa c*-551 (PBD 351C[11]). Residue 13 and 22 mutants of *Ht c*-552, and residue 7 mutants of both proteins, are analyzed herein.

influence heme ruffling in both proteins,[11,16,17] and mutations of residues 13 and 22 have been shown to affect the His−Fe(III) interaction and are proposed to influence heme ruffling.[18,19]

Ruffling is typically the dominant mode of out-of-plane distortion for heme *c*[21] and can be envisioned as twisting along the Fe−N(pyrrole) bonds in alternate directions (Figure 4).[22] The X-ray crystal structure of the Phe7Ala mutant of *Pa c*-551 (*Pa*F7A)[17] indicates an increase in the out-of-plane displacement along the ruffling coordinate of 0.4 Å measured using normal coordinate structural decomposition analysis[16,22] of the X-ray crystal structures of *Pa c*-551[11] and *Pa*F7A.[17] The basis for the change in ruffling may be the shortening of the

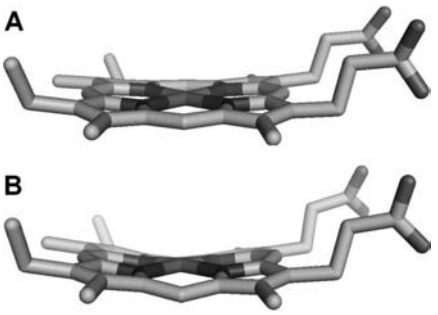

Figure 4. Structure of the heme from (A) *Pa c*-551 (PBD 351C),[11] 0.49 Å ruffling, and (B) *Pa*F7A (PBD 2EXV),[20] 0.86 Å ruffling. Normal coordinate structure decomposition[22] was used to evaluate amount of ruffling.

hydrogen bond between the residue 7 backbone carbonyl oxygen and Cys12 amide NH in *Pa*F7A relative to wild-type.[16,17] Conversely, NMR analysis has revealed that the A7F mutation in *Ht c*-552 decreases heme ruffling by ∼0.1 Å.[16] The M13V and K22M mutations in *Ht c*-552 have been demonstrated to increase His-Fe(III) bond strength, and have been proposed although not proven to influence heme ruffling.[18,19] These variants span an 80-mV range of E_m, corresponding to an increase in His−Fe(III) bond strength as E_m decreases (*Ht c*-552, 236 ± 2 mV; *Ht*K22M, 199 ± 1; *Ht*M13V, 177 ± 1 mV; *Ht*M13V/K22M, 155 ± 2 mV).[18] Position 7, 13, and 22 variants of *Ht c*-552 and position 7 variants of *Pa c*-551 are used here for a detailed investigation of the effects of His-Fe(III) bonding and heme ruffling on the electronic structure of heme proteins with His-Met axial ligation as revealed by EPR spectroscopy.

EXPERIMENTAL SECTION

Protein Expression and Purification. Expression of *Ht c*-552,[23] *Ht*M13V, *Ht*K22M, *Ht*M13V/K22M,[18] and *Ht*A7F[16] was in *E. coli* BL21(DE3)Star (Invitrogen) containing pEC86 for overexpression of the *E. coli* cytochrome *c* maturation genes[24] and the appropriate cytochrome *c* expression plasmid harboring the cytochrome structural gene with a signal sequence. The expression plasmids for *Ht c*-552 and variants are based on pET17b (Amp^r) (Novagen) and utilize a modified N-terminal signal sequence from *Thiobacillus versutus* cytochrome c_{550} to direct secretion of the apoprotein to periplasm for maturation.[25] Purification was as described.[18] Expression of *Pa c*-551 and *Pa*F7A also was in *E. coli* BL21(DE3)Star and used a pET17b-based plasmid containing the *Pa c*-551 gene along with its native signal sequence[20,26] in addition to pEC86. The QuikChange II site-directed mutagenesis kit (Stratagene) was used to prepare the F7A variant of *Pa c*-551. Purification of *Pa c*-551 and *Pa*F7A was as described[27] and yielded 15−20 mg protein/L of medium.

EPR Spectroscopy. EPR measurements on cytochrome *c* variants (protein concentration 200−300 μM, 50 mM HEPES, pH 7.5) were carried out in a dual-band X-cavity on a Bruker Elexsys 500E spectrometer characterized by a cavity quality factor (Q) > 4000 and equipped with a He−flow cryostat (ESR 900, Oxford Instruments). Spectra were recorded at a temperature of 9.0 ± 1.0 K and a microwave frequency of 9.663(8) GHz. To avoid saturation effects, the microwave power was calibrated for each protein sample and all EPR spectra reported here were obtained with a microwave power well below $P_{1/2}$. Microwave powers used were as follows: *Ht c*-552, 1.0 mW; *Ht*K22M, 6.4 mW; *Ht*M13V, 3.2 mW; *Ht*MI3V/K22M, 0.63 mW; *Pa c*-551, 1.0 mW; *Pa*F7A, 3.6 mW. Spectra were collected with a modulation amplitude of 0.7 mT, modulation frequency of 100 kHz, gain of 57 dB, sweep time of 168−335 s, and time constant of 82−164 ms. For each sample, 2−6 scans were accumulated and averaged. EPR spectra were baseline corrected by subtraction of a scan of the cavity

dx.doi.org/10.1021/ic201479q | *Inorg. Chem.* 2011, 50, 12018−12024

Table 1. *g*- and Ligand-Field (V, Δ) Values Derived from Low-Temperature X-Band EPR Experiments[a]

	g_{max}	g_{mid}	g_{min}	rhombic term V/λ	axial term Δ/λ	rhombicity V/Δ
Ht c-552	3.23	2.04	1.19	1.23 ± 0.02	3.41 ± 0.06	0.36 ± 0.01
*Ht*K22M	3.23	2.08	1.19	1.24 ± 0.02	3.23 ± 0.08	0.38 ± 0.01
*Ht*M13V	3.19	2.09	1.17	1.26 ± 0.02	3.06 ± 0.10	0.41 ± 0.01
*Ht*M13V/K22M	3.17	2.11	1.17	1.28 ± 0.01	2.96 ± 0.06	0.43 ± 0.01
Ht c-552	3.20[b]	2.08[b]	1.20[b]	1.3 ± 0.1[b]	3.2 ± 0.2[b]	0.39 ± 0.07[b]
*Ht*A7F	3.17[b]	2.10[b]	1.24[b]	1.3 ± 0.1[b]	3.3 ± 0.2[b]	0.41 ± 0.07[b]
Pa c-551	3.20[b]	2.06[b]	1.23[b]	1.28 ± 0.02[b]	3.45 ± 0.03[b]	0.37 ± 0.01[b]
*Pa*F7A	3.15	2.09	1.15	1.26 ± 0.02	2.94 ± 0.05	0.43 ± 0.01

[a]The symbol λ indicates the spin-orbit coupling constant (~400 cm^{-1}). [b]Data taken from ref 9–16.

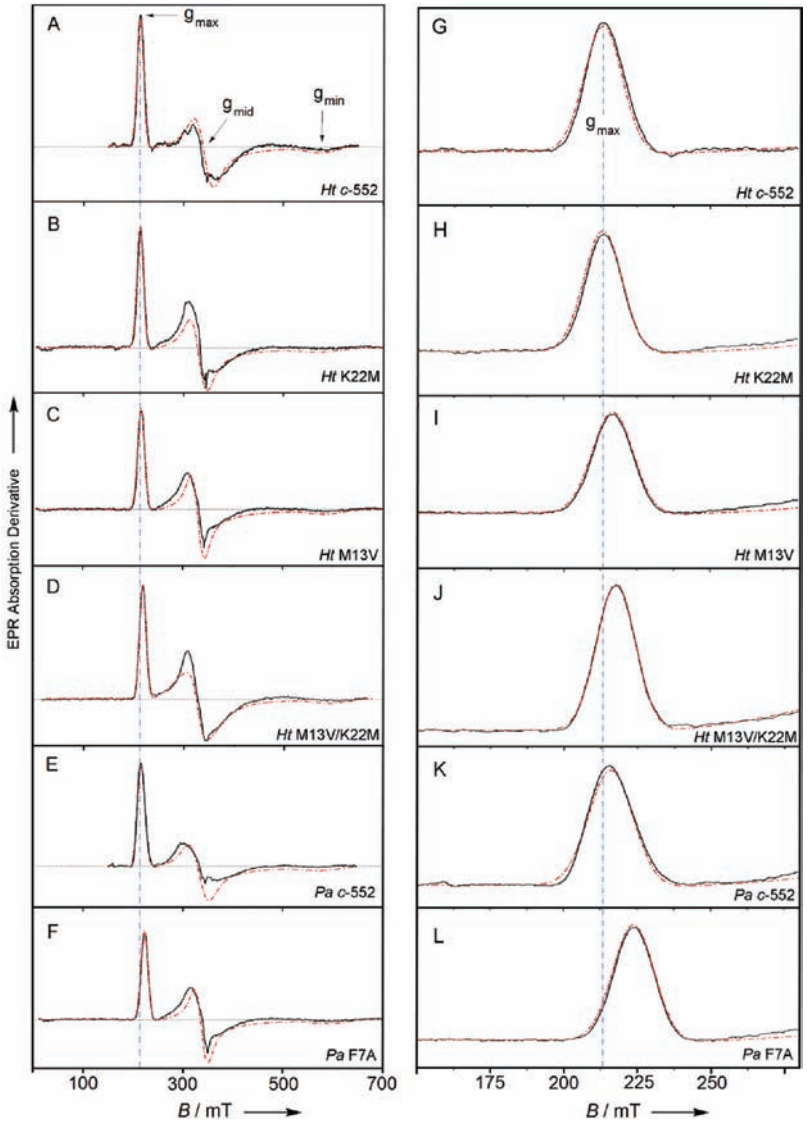

Figure 5. X-band EPR spectra of variants of *Ht c*-552 and *Pa c*-551: (A,G) *Ht c*-552, (B,H) *Ht*K22M, (C,I) *Ht*M13V, (D,J) *Ht*MI3V/K22M, (E,K) *Pa c*-551, (F,L) *Pa*F7A. Sample concentration was 200–300 μM protein in 50 mM HEPES, pH 7.5. Measurements were performed at a temperature of 9.0 ± 1.0 K. The dashed red lines represent simulated EPR envelopes. The dashed blue line is a guide to the eye and indicates the g_{max} value for *Ht c*-552. Panels G–L are expansions of the g_{max} line.

and the EPR tube containing buffer (keeping the same filling volume) recorded under identical conditions. The EPR simulation platform XSophe (version 1.1.3) and XeprView (version 1.2b.33) software were provided by Bruker.[28]

Determination of Ligand–Field Parameters. The ligand–field correlation analysis employed in this work follows the formalism introduced by Griffith[29,30] and developed by Taylor.[15] Axial (Δ/λ) and rhombic (V/λ) ligand-field terms (Figure 2) were determined from the experimental g values according to the following equations:

$$\frac{V}{\lambda} = \frac{E_{yz}}{\lambda} - \frac{E_{xz}}{\lambda} = \frac{g_{xx}}{g_{zz} + g_{yy}} + \frac{g_{yy}}{g_{zz} + g_{xx}} \quad (1)$$

dx.doi.org/10.1021/ic201479q | *Inorg. Chem.* 2011, 50, 12018–12024

$$\frac{\Delta}{\lambda} = \frac{E_{yz}}{\lambda} - \frac{E_{xy}}{\lambda} - \frac{V}{2\lambda} = \frac{g_{xx}}{g_{zz} + g_{yy}} + \frac{g_{zz}}{g_{yy} - g_{xx}} - \frac{V}{2\lambda} \quad (2)$$

Use of these equations requires that the normalization condition holds:[15,31]

$$g_{xx}^2 + g_{yy}^2 + g_{zz}^2 + g_y g_z - g_x g_z - g_x g_y - 4(g_{zz} + g_{yy} - g_{xx}) = 0 \quad (3)$$

The spectra of the cytochrome *c* variants studied in this work fulfill the conditions expressed by eq 3. The calculated orbital coefficient values (*a*, *b*, *c*) and details of the procedure employed for estimation of errors in the ligand–field terms are provided in the Supporting Information.

RESULTS

The experimentally determined *g*-tensor components and the derived ligand-field terms for the proteins in this study are presented in Table 1. The EPR spectra of all of the protein variants exhibit resonance signals consistent with low-spin ($S = 1/2$) ferric heme with a $(d_{xy})^2(d_{xz},d_{yz})^3$ electronic configuration and moderate rhombic distortion (Figure 5, Supporting Information Figure S2, Table 1). For the *Ht* *c*-552 position 13 and 22 variants, a linear relationship between V/λ and Δ/λ values and E_m (Figure 6) is observed. The position 13 and 22

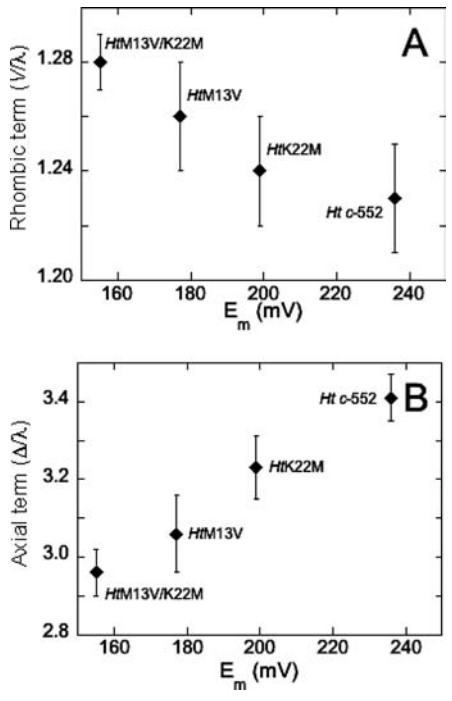

Figure 6. Correlation between midpoint potentials and (A) V/λ and (B) Δ/λ, for *Ht* *c*-552 and its position 13 and 22 variants.

variants of *Ht* *c*-552 show a linear increase in the rhombic term V/λ and decrease in the axial term Δ/λ as E_m decreases; both factors contribute to the increase of rhombicity (V/Δ) over the series. However, the variation in V/λ values is relatively small, thus changes in Δ/λ dominate the d-orbital distribution. *Ht*A7F, in contrast, shows minimal change in its EPR spectrum relative to wild-type.[16] *Pa*F7A exhibits a slightly higher rhombicity in comparison with *Pa* *c*-551, but with a larger change in Δ/λ than in V/λ (Table 1).

DISCUSSION

The axial His-Fe(III) bond strength is proposed to be related to the amount of anionic (histidinate) character of the axial His which influences the reduction potential of peroxidases[32] and cytochromes.[19] For a given His orientation, histidinate character also is related to the strength of the hydrogen bond between the axial His δ1 NH and its hydrogen bond acceptor, which in cytochromes *c* is a proline carbonyl. Because a stronger bond from His to Fe(III) stabilizes the higher oxidation state, reduction potential will decrease with increasing His–Fe(III) bond strength. Accordingly, the position 13 and 22 mutants of *Ht* *c*-552 have been shown to have a stronger His–Fe(III) bond as E_m is lowered. Note that these mutations have been shown to have a minimal effect on the properties of the Fe(II) state of *Ht* *c*-552.[19] The His–Fe(III) and Met–Fe(III) interactions have significant σ-bonding character involving the Fe d_{z2} orbital. The predicted effect of enhanced σ-bonding between axial ligands and the iron is to increase the energy of the d_{z2} orbital, as illustrated in Figure 7A. The Fe d_{xz}

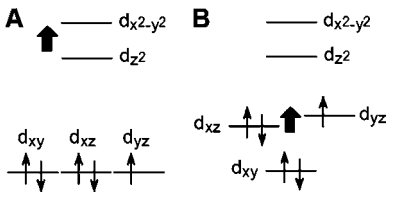

Figure 7. Effects of enhanced (A) σ donation and (B) π donation to iron on the relative energies of the Fe(III) d orbitals.

and d_{yz} orbitals exhibit π-interactions with the Met δS lone pair, the porphyrin π-system, and the His π orbitals. Enhancing π interactions with the Fe d_{xz} and d_{yz} orbitals will raise their energies as shown in Figure 7B. Preferential destabilization of either the d_{xz} or d_{yz} orbital as Fe(III)-ligand π-bonding depends on the orientations of the axial ligands relative to the heme *x*, *y* plane.

His–Fe(III) Bonding. Analysis of the EPR spectra of the position 13 and 22 variants reveals that the rhombic term V/λ, reflecting the difference in energy between the d_{xz} and d_{yz} orbitals, shows a small increase across the series: *Ht* *c*-552 < *Ht*K22M < *Ht*M13V < *Ht*M13V/K22M (i.e., from higher to lower E_m), whereas Δ/λ decreases. Can these changes be attributed to the effects of increasing His–Fe(III) bond strength that was previously established?[19] The axial His is nearly aligned with the α,γ-meso carbons of the heme (Figure 1A).[11,17] Changes in the Fe(III)–His bond strength observed across this series thus are expected to affect the d_{xz} and d_{yz} energies similarly. The small amount of change in V/λ with increasing His–Fe(III) bond strength is consistent with the His being nearly, but not precisely, aligned with the α,γ-meso carbons (Figure 1A), because increasing the bond strength will result in more overlap between the π-system of the His with *both* the d_{xz} and d_{yz} orbitals, raising both energies to a similar extent. As a result, an increase in the axial His-Fe(III) interaction in this system is predicted to increase the axial term Δ/λ but exert little change on the rhombic term V/λ. However, we observe a *decrease* in the axial term with increasing His–Fe(III) bond strength. To explain this trend, we next

dx.doi.org/10.1021/ic201479q | *Inorg. Chem.* 2011, 50, 12018–12024

consider the effects of variation of heme ruffling on electronic structure.

Heme Ruffling. The *Pa c*-551/*Pa*F7A and the *Ht c*-552/*Ht*A7F wild-type/mutant pairs are valuable for examining the effect of heme ruffling on ligand-field parameters as they exhibit changes in ruffling that have been established previously.[16] EPR results for the *Ht c*-552/*Ht*A7F pair and for *Pa c*-551 were reported elsewhere[9,16] and the EPR spectrum for *Pa*F7A is reported here. Comparison of EPR results for *Pa c*-551 and *Pa*F7A shows that the rhombic term V/λ does not change upon mutation whereas the axial term Δ/λ decreases significantly for the more ruffled F7A mutant. In Taylor's model for the $(d_{xy})^2(d_{xz},d_{yz})^3$ configuration, $\Delta/\lambda = 1/2(E_{xz} + E_{yz}) - E_{xy}$, hence a decrease in Δ/λ reflects either (1) a decrease in the d_{xz},d_{yz} orbital energies (E_{xz} and E_{yz}) relative to E_{xy} or (2) an increase in E_{xy} relative to E_{xz} and E_{yz}; a combination of these effects also is possible. In Taylor's treatment, the $S = 1/2$ wave functions ($|+\rangle$, $|-\rangle$) are described as a weighted admixture of the d_{xy}, d_{xz}, and d_{yz} orbitals with orbital coefficients *a*, *b*, and *c*

$$|+\rangle = a|d_{yz}^{+}\rangle - ib|d_{xz}^{+}\rangle - c|d_{xy}^{-}\rangle$$

$$|-\rangle = -a|d_{yz}^{-}\rangle - ib|d_{xz}^{-}\rangle - c|d_{xy}^{+}\rangle$$

By utilizing the normalization condition $\Sigma(a)^2 + (b)^2 + (c)^2 = 1.00 \pm 0.01$ we can determine the coefficients for the d_{xy}, d_{xz}, and d_{yz} components of the three-orbitals-one-hole wave functions. The result for *Pa c*-551 is that the spin functions contain ~86% d_{yz}, 12% d_{xz}, and 2% d_{xy} while in *Pa*F7A they contain ~85% d_{yz}, 12% d_{xz}, and 3% d_{xy}. Thus the contributions of both the d_{yz} and d_{xy} orbitals are altered by mutation, although the d_{xy} has the larger relative change.

The influence of heme conformation on the d orbital energies is mediated by interactions between the filled $3e(\pi)$ porphyrinate orbital and the d_{xz} and d_{yz} ($d(\pi)$) metal orbitals, and, if the macrocycle is ruffled, by interactions between the filled $3a_{2u}(\pi)$ porphyrinate orbital and the d_{xy} orbital (Figure 8).

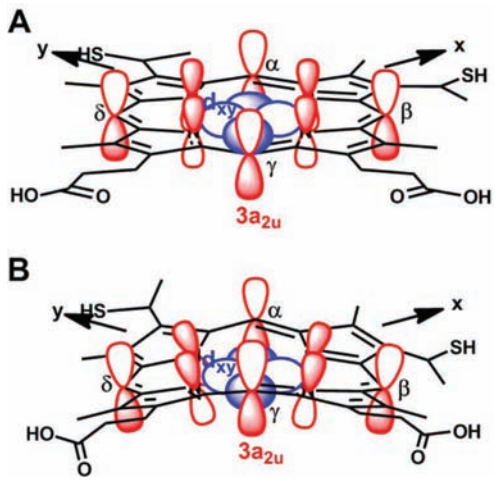

Figure 8. Illustration of the $3a_{2u}$ orbital and the d_{xy} orbital in (A) planar heme (interaction not allowed) and (B) ruffled heme (interaction allowed).

Those interactions depend on the relative energies of the $d(\pi)$ metal and $e(\pi)$ macrocycle frontier orbitals. Thus, the smaller axial term (Δ/λ) may indicate either (1) a weakening of the $3e(\pi)$–$d(\pi)$ interaction in *Pa*F7A with respect to *Pa c*-551 to lower E_{yz}, or (2) an enhanced interaction between $3a_{2u}(\pi)$ and d_{xy} to raise E_{xy}; a combination of these factors also is possible. From CW-EPR data alone, we cannot determine which of these is the major contributor. In a recent DFT study, however, an increase in heme ruffling in low-spin heme with His/Met axial ligation was predicted to increase the energies of all three t_{2g}-derived orbitals, although the effect was much more pronounced for d_{xy}. The DFT predictions were validated by NMR spectroscopy performed on *Ht c*-552 and on *Ht*-A7F; the results demonstrated that the mutation decreases heme ruffling.[16]

In contrast with the *Pa c*-551/PaF7A pair, *Ht*A7F displays no significant difference in ligand-field terms from *Ht c*-552. EPR data are consistent with a small increase in Δ/λ for *Ht*A7F, however, the change is within the margin of error. The small change in Δ/λ for *Ht*A7F relative to wild-type may be attributed to the very small change in ruffling seen between these proteins (~0.1 Å, determined by NMR)[16] relative to the *Pa c*-551/*Pa*F7A pair (~0.4 Å, measured from crystal structures).[11,17] Thus, EPR may be sensitive to moderate or large heme ruffling differences between hemes with His/Met axial ligation although it may not reflect small heme ruffling changes that are detectable by NMR.[16]

As noted above, Δ/λ decreases across the series *Ht c*-552 > *Ht*K22M > *Ht*M13V > *Ht*M13V/K22M as E_m decreases, although an increase in the axial His-Fe(III) bond strength is predicted to result in an *increase* in the axial term Δ/λ. This result thus supports the hypothesis that heme ruffling increases across this series of variants with decreasing E_m, resulting in a higher energy for d_{xy} and a lower Δ/λ. The average value of the heme methyl chemical shifts shows an established trend with a change in ruffling, and the average heme methyl ^{1}H chemical shift decreases across the series of position 13 and 22 *Ht c*-552 mutants as E_m decreases, consistent with an increase in heme ruffling.[16,19,33] The average heme methyl chemical shift also is sensitive to axial ligand donor properties. As the axial His becomes a better donor (more histidinate character), the average heme methyl shift moves upfield as a result of a decrease in porphyrin-to-Fe(π) spin delocalization as the His-to-Fe(III) σ-interaction increases.[34] Thus both an increase in heme ruffling and in His-donor properties may be causes of the observed trend in heme methyl chemical shifts. However, as enhanced His-Fe(III) bonding is predicted to increase Δ/λ, we conclude that the differences observed in the EPR spectra among the variants arise primarily from differences in ruffling.

Structural Basis for Ruffling and Functional Implications. A clue to the structural basis for the trend in heme ruffling in the position 13 and 22 mutants may be found in the previously reported effects of these mutations on the CXXCH pentapeptide. The M13V and K22M mutations were previously proposed to enhance packing on the proximal (axial His) side of the heme. Accordingly, these mutations were found to increase the rigidity of the proximal heme pocket. The backbone HN protons of Cys15 and His16 hydrogen bond with the Cys12 carbonyl oxygen (Figure 9), and the persistence of these interactions has been probed by hydrogen–deuterium exchange NMR.[18] In *Ht*M13V, *Ht*K22M, and *Ht*M13V/K22M, the backbone HN protons of Cys15 and His16 show increased protection from exchange with solvent, with amount of protection generally increasing as E_m decreases.[18] This result is interpreted to indicate a more locally stable or rigid CXXCH peptide backbone in the lower-potential mutants with enhanced polypeptide packing near the axial His. Studies of micro-peroxidase heme peptides derived from horse cytochrome *c*

dx.doi.org/10.1021/ic201479q | *Inorg. Chem.* 2011, 50, 12018–12024

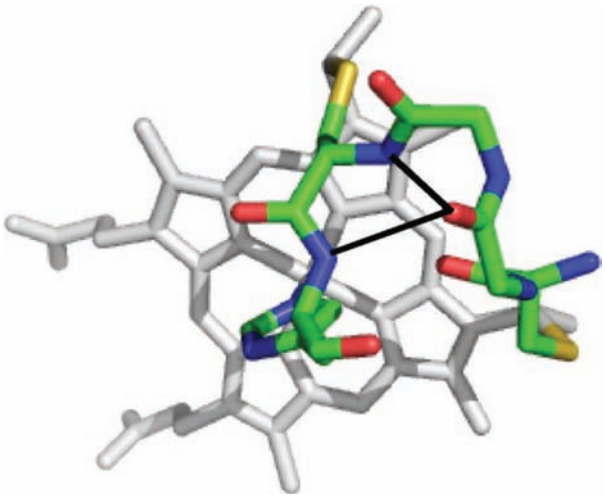

Figure 9. Structure of the heme and the residues 12−16 in *Ht c*-552 (PDB 1YNR).[20] The hydrogen-bonding interactions from Cys12(CO) to Cys15(HN) and His16 (HN) proposed to play a role in modulating CXXCH rigidity and heme ruffling are shown with black lines. The side chains of residues 13 and 14 are omitted for clarity.

have previously demonstrated that strengthening hydrogen bonding within the CXXCH segment enhances heme ruffling.[35] Thus, we propose that enhanced hydrogen bonding within the CXXCH pentapeptide backbone contributes to increasing heme ruffling in these mutants.

Across the series of position 13 and 22 mutants, moving from higher to lower E_m, we propose that both heme ruffling and His-Fe(III) bond strength are enhanced. Might axial bond strength and heme ruffling be linked to each other? The effect of heme ruffling on axial bond strength has been explored in a study of ligand-binding affinities of ferric myoglobins reconstituted with heme derivatives showing different amounts of ruffling. Heme distortion is proposed to increase the Fe(III)-His bond strength in that work.[36] In contrast, DFT calculations on a Met-His-coordinated heme predict a negligible effect of heme ruffling on Fe(III)−His bond length with a bond length change of less than 0.001 Å upon a change of ruffling of 0.7 Å (see Supporting Information of ref 16). However, it is possible that protein structure-related factors affecting heme ruffling also directly affect the Fe(III)−His bond strength, or that changes in ruffling and bond strength are otherwise related to each other. In contrast with the analyses of Fe(III)−His bonding, a study of dioxygen binding to the highly distorted ferrous heme in *Methanosarcina acetivorans* protoglobin indicates that out-of-plane distortions decrease dioxygen affinity, whereas in-plane distortions may increase or decrease affinity.[37] Consistent with the conclusions on protoglobin, a study of the effect of heme ruffling on ligand-binding to *Thermoanaerobacter tencongenesis* heme nitric oxide/oxygen binding domain suggests that flattening of the heme increases the proximal bond strength of the Fe(II)−O_2 complex.[38] How ruffling affects axial ligand interactions remains a question for further research, but likely depends on heme oxidation state, electronic structure, and the nature of the ligand(s).

In a previous study, changes in heme ruffling were proposed to influence whether highly axial low-spin (HALS)-type (high g_{max}) or rhombic EPR spectra of Met-His coordinated cytochromes *c* were observed.[9] The analysis here indicates a limited effect of heme ruffling on g_{max}. A g_{max} value difference of only 0.05 is observed between *Pa c*-551 and *Pa*F7A despite the 0.4-Å change in the heme ruffling; the difference between the g_{max} values of wild-type *Ht c*-552 and *Ht*M13V/K22M, the variant with the greatest difference in E_m from wild-type, is only 0.06. Thus, changes exerted on EPR spectra by heme ruffling in these systems can not be the sole basis for the large range of g_{max} values exhibited by cytochromes.[10] However, it is notable that *Bacillus pasteurii* cytochrome c_{553} has a low amount of ruffling for a cytochrome *c* (0.36 Å)[39] and a large g_{max} signal (3.36).[8]

There has been considerable interest in the question of the functional relevance of covalent heme attachment in cytochromes *c*.[1,40,41] One proposal is that covalent attachment provides means by which redox potential may be tuned, as hemes *c* display a wider range of potentials in nature than hemes *b*, which bind the polypeptide through coordinate bonds and noncovalent interactions.[1,42] The observation that mutations in and near the CXXCH motif influence heme ruffling and His-Fe(III) bonding, supports the hypothesis that covalent attachment, the identity of the variable residues within this motif, and interactions with this motif influence heme conformation, and thus heme *c* redox potential.

■ ASSOCIATED CONTENT

Ⓢ Supporting Information

Detailed description of the determination of ligand-field parameters from *g*-values and their errors, error distribution in the *g*-tensor and calculated ligand-field parameters (5 tables), an illustration of the error analysis procedure and an expansion of the high-field region of EPR spectra of the protein variants with fits (2 figures). This material is available free of charge via the Internet at http://pubs.acs.org.

■ AUTHOR INFORMATION

Corresponding Author

*E-mail: bren@chem.rochester.edu.

Author Contributions

[§]These authors contributed equally.

■ ACKNOWLEDGMENTS

This work was supported by The National Institutes of Health (NIH) of the United States of America Grant GM63170 (K.L.B.), the Research Council of Norway Grant 177661/V30 (K.K.A.). G.Z. thanks the PEOPLE Marie Curie actions Intra European Fellowship within the seventh European Community Framework Program (PIEF-GA-2009-235237) for support.

■ REFERENCES

(1) Bowman, S. E. J.; Bren, K. L. *Nat. Prod. Rep.* **2008**, *25*, 1118−1130.

(2) Reedy, C. J.; Elvekrog, M. M.; Gibney, B. R. *Nucleic Acids Res.* **2008**, *36*, D307−D313.

(3) Fufezan, C.; Zhang, J.; Gunner, M. R. *Proteins* **2008**, *73*, 690−704.

(4) Senn, H.; Keller, R. M.; Wüthrich, K. *Biochem. Biophys. Res. Commun.* **1980**, *92*, 1362−1369.

(5) Moore, G. R.; Pettigrew, G. W. *Cytochromes c; Evolutionary, Structural, and Physicochemical Aspects*; Springer-Verlag: Berlin, 1990.

(6) Zhong, L.; Wen, X.; Rabinowitz, T. M.; Russell, B. S.; Karan, E. F.; Bren, K. L. *Proc. Natl. Acad. Sci. U.S.A.* **2004**, *101*, 8637−8642.

(7) Bren, K. L.; Kellogg, J. A.; Kaur, R.; Wen, X. *Inorg. Chem.* **2004**, *43*, 7934−7944.

(8) Zoppellaro, G.; Teschner, T.; Harbitz, E.; Schuenemann, V.; Karlsen, S.; Arciero, D. M.; Ciurli, S.; Trautwein, A. X.; Hooper, A. B.; Andersson, K. K. *ChemPhysChem* **2006**, *7*, 1258−1267.

(9) Zoppellaro, G.; Harbitz, E.; Kaur, R.; Ensign, A. A.; Bren, K. L.; Andersson, K. K. *J. Am. Chem. Soc.* **2008**, *130*, 15348−15360.
(10) Zoppellaro, G.; Bren, K. L.; Ensign, A. A.; Harbitz, E.; Kaur, R.; Hersleth, H. P.; Ryde, U.; Hederstedt, L.; Andersson, K. K. *Biopolymers* **2009**, *91*, 1064−1082.
(11) Matsuura, Y.; Takano, T.; Dickerson, R. E. *J. Mol. Biol.* **1982**, *156*, 389−409.
(12) Walker, F. A. *Chem. Rev.* **2004**, *104*, 589−615.
(13) Bertini, I.; Luchinat, C.; Parigi, G.; Walker, F. A. *J. Biol. Inorg. Chem.* **1999**, *4*, 515−519.
(14) Shokhirev, N. V.; Walker, F. A. *J. Biol. Inorg. Chem.* **1998**, *3*, 581−594.
(15) Taylor, C. P. S. *Biochim. Biophys. Acta* **1977**, *491*, 137−149.
(16) Liptak, M. D.; Wen, X.; Bren, K. L. *J. Am. Chem. Soc.* **2010**, *132*, 9753−9763.
(17) Borgia, A.; Bonivento, D.; Travaglini-Allocatelli, C.; Di Matteo, A.; Brunori, M. *J. Biol. Chem.* **2006**, *281*, 9331−9336.
(18) Michel, L. V.; Ye, T.; Bowman, S. E. J.; Levin, B. D.; Hahn, M. A.; Russell, B. S.; Elliott, S. J.; Bren, K. L. *Biochemistry* **2007**, *46*, 11753−11760.
(19) Bowman, S. E. J.; Bren, K. L. *Inorg. Chem.* **2010**, *49*, 7890−7897.
(20) Travaglini-Allocatelli, C.; Gianni, S.; Dubey, V. K.; Borgia, A.; Di Matteo, A.; Bonivento, D.; Cutruzzolà, F.; Bren, K. L.; Brunori, M. *J. Biol. Chem.* **2005**, *280*, 25729−25734.
(21) Hobbs, J. D.; Shelnutt, J. A. *J. Protein Chem.* **1995**, *14*, 19−25.
(22) Jentzen, W.; Song, X. Z.; Shelnutt, J. A. *J. Phys. Chem. B* **1997**, *101*, 1684−1699.
(23) Karan, E. F.; Russell, B. S.; Bren, K. L. *J. Biol. Inorg. Chem.* **2002**, *7*, 260−272.
(24) Arslan, E.; Schulz, H.; Zufferey, R.; Kunzler, P.; Thöny-Meyer, L. *Biochem. Biophys. Res. Commun.* **1998**, *251*, 744−747.
(25) Fee, J. A.; Chen, Y.; Todaro, T. R.; Bren, K. L.; Patel, K. M.; Hill, M. G.; Gomez-Moran, E.; Loehr, T. M.; Ai, J. Y.; Thony-Meyer, L.; Williams, P. A.; Stura, E.; Sridhar, V.; McRee, D. E. *Protein Sci.* **2000**, *9*, 2074−2084.
(26) Wen, X.; Bren, K. L. *Inorg. Chem.* **2005**, *44*, 8587−8593.
(27) Russell, B. S.; Zhong, L.; Bigotti, M. G.; Cutruzzolà, F.; Bren, K. L. *J. Biol. Inorg. Chem.* **2003**, *8*, 156−166.
(28) Hanson, G. R.; Gates, K. E.; Noble, J. C.; Griffin, M.; Mitchell, A.; Benson, S. *J. Inorg. Biochem.* **2004**, *98*, 903−916.
(29) Griffith, J. S. *Nature* **1957**, *180*, 30−31.
(30) Griffith, J. S. *Mol. Phys.* **1971**, *21*, 135−139.
(31) Castner, T. J. Jr. *Phys. Rev.* **1959**, *115*, 1506−1515.
(32) Poulos, T. L. *J. Biol. Inorg. Chem.* **1996**, *1*, 356−359.
(33) Shokhireva, T. K.; Shokhirev, N. V.; Berry, R. E.; Zhang, H. J.; Walker, F. A. *J. Biol. Inorg. Chem.* **2008**, *13*, 941−959.
(34) Chacko, V. P.; Lamar, G. N. *J. Am. Chem. Soc.* **1982**, *104*, 7002−7007.
(35) Ma, J. G.; Vanderkooi, J. M.; Zhang, J.; Jia, S. L.; Shelnutt, J. A. *Biochemistry* **1999**, *38*, 2787−2795.
(36) Neya, S.; Suzuki, M.; Hoshino, T.; Ode, H.; Imai, K.; Komatsu, T.; Ikezaki, A.; Nakamura, M.; Furutani, Y.; Kandori, H. *Biochemistry* **2010**, *49*, 5642−5650.
(37) Bikiel, D. E.; Forti, F.; Boechi, L.; Nardini, M.; Javier Luque, F.; Martí, M. A.; Estrin, D. A. *J. Phys. Chem. B* **2010**, *114*, 8536−8543.
(38) Olea, C.; Boon, E. M.; Pellicena, P.; Kuriyan, J.; Marletta, M. A. *ACS Chem. Biol.* **2008**, *3*, 703−710.
(39) Benini, S.; Gonzalez, A.; Rypniewski, W. R.; Wilson, K. S.; Van Beeumen, J. J.; Ciurli, S. *Biochemistry* **2000**, *39*, 13115−13126.
(40) Stevens, J. M.; Daltrop, O.; Allen, J. W. A.; Ferguson, S. J. *Acc. Chem. Res.* **2004**, *37*, 999−1007.
(41) Allen, J. W. A.; Barker, P. D.; Daltrop, O.; Stevens, J. M.; Tomlinson, E. J.; Sinha, N.; Sambongi, Y.; Ferguson, S. J. *Dalton Trans.* **2005**, 3410−3418.
(42) Zheng, Z.; Gunner, M. R. *Proteins* **2009**, *75*, 719−734.